Myosin 1b Flattens and Prunes Branched Actin Filaments.

Julien Pernier[1,2,3], Antoine Morchain[1,2], Valentina Caorsi[4], Aurélie Bertin[1,2], Hugo Bousquet[2,3], Patricia Bassereau[1,2*], Evelyne Coudrier[2,3*]

1. Laboratoire Physico-Chimie Curie, Institut Curie, PSL Research University, CNRS UMR168, 75005 Paris, France
2. Sorbonne Université, 75005 Paris, France
3. Institut Curie, PSL Research University, C.N.R.S. UMR 144, 26 rue d'Ulm, Paris, France
4. Abbelight, 191 avenue Aristide Briand, 94230 Cachan, France

*: corresponding authors: patricia.bassereau@curie.fr and evelyne.coudrier@curie.fr

Abstract

Motile and morphological cellular processes require a spatially and temporally coordinated branched actin network that is controlled by the activity of various regulatory proteins including the Arp2/3 complex, profilin, cofilin and tropomyosin. We have previously reported that myosin 1b regulates the density of the actin network in the growth cone. Using *in vitro* F-actin gliding assays and total internal reflection fluorescence (TIRF) microscopy we show in this report that this molecular motor flattens the Arp2/3-dependent actin branches up to breaking them and reduces the probability to form new branches. This experiment reveals that myosin 1b can produce force sufficient enough to break up the Arp2/3-mediated actin junction. Together with the former *in vivo* studies, this work emphasizes the essential role played by myosins in the architecture and in the dynamics of actin networks in different cellular regions.

Keywords

Myosin 1b, Myosin 2, branched actin, Arp2/3, gliding assay, TIRF microscopy, actin architecture

Results and Discussion

Numerous motile and morphological processes require a spatially and temporally coordinated branched actin -filament (F-actin) network. Polymerization and assembly of this branched F-actin network are controlled by the activity of various regulatory proteins including the Arp2/3 complex [1], profilin [2], cofilin [3] and tropomyosin [4]. In addition of these regulatory actin binding proteins, several myosin motors have been reported to control actin architecture, either bound to cell membranes such as myosins 1 (see below), 6 [5-7] and 10 [8] or associated to actin filaments only such as myosin 2 [5]. For instance, studies in Xenopus oocytes suggest that myosin 1c and myosin 1e control cortical granule exocytosis and the subsequent compensatory endocytosis by directly regulating actin polymerization [9-11]. In *S cerevisiae,* myosin 1 (Myo5) induces actin polymerisation depending on the Arp2/3 complex [12, 13]. We have previously reported that a mammalian myosin 1, myosin 1b (Myo1b) limits the extension of the actin network in the growth cones of the cortical neurons [14] and moreover, depolymerizes F-actin at the barbed end [15]. In this work we have investigated the potential impact of Myo1b on the architecture and on the dynamics of branched F-actin networks.

Myo1b is a single-headed motor composed of three domains: a N terminal motor domain that coordinates ATP hydrolysis, actin binding and force generation, a light chain binding domain (LCBD) that binds calmodulin, and a tail region with a highly basic C-terminal tail homology 1 (TH1) [16] (Fig. 1A). In contrast to the non-muscle myosin II a pleckstrin homology (PH) motif in the TH1 domain targets Myo1b to phosphoinositides in the membrane [17] (Fig. 1A). In contrast to Myo2, Myo1b is a catch-bond motor, i.e. the time Myo1b remains bound to F-actin strongly increases with a pN force [18].

In this paper, we have used *in vitro* F-actin gliding assays and total internal reflection fluorescence (TIRF) microscopy to study the effect of full-length Myo1b on stabilized (I) and polymerizing (II) branched F-actin, when immobilized on a solid substrate (Fig. 1B).

Branch density of stabilized F-actin decreases when sliding on Myo1b

We first polymerized actin filaments in solution, in the presence of the constitutively active C-terminal domain of N-WASP (VCA) and Arp2/3 complex (STAR Methods) in similar experimental conditions as described by Pernier and colleagues [2], to generate branched filaments and stabilize them with phalloidin. We analyzed the filaments' architecture and movement when they slide on Myo1b bound to the glass substrate at a density of about 8000/μm^2 (Fig. 1C, movie S1). In the absence of Myo1b and with the same surface treatment, the branches are stable over time, at least up to 10 minutes (Movie S1, Figs. 1C and 1E). In contrast, when the filaments slide on the motors, we observe large variations of the orientation of the branches relative to the mother filaments, already visible 1 or 2 minutes after filaments glide on Myo1b (Movie S1 and Fig. 1C) and in some cases, we observe detachment of branches from the mother at the level of the branch attachment (Movie S1 and Fig. 1C, last frames). The distribution of actin filament length after 160 sec shows many more shorter filaments when gliding on Myo1b (Fig. 1D), while keeping the total length conserved as compared to the initial frame and to the control. This confirms that Myo1b detaches the branches. As a comparison, we used another myosin, the muscle myosin II (Myo2) that leads to a five-fold faster linear F-actin sliding [15]. At the same surface density (about 8000/μm^2), we did not observe branches on filaments gliding on Myo2, but actin

filament fragments, likely due to a fast detachment occurring before image acquisition starts, i.e. one minute after injection of stabilized branched filaments in the chamber (Movie S2). Since we aim at characterizing the details of the debranching process by myosins, we focus on Myo1b in the following, given the time scale of our experiments.
We have next quantified the relative variation of the number of branches along actin filaments over time. We observe an important decrease of the number of branches, by about five-fold within 3 minutes for Myo1b (Fig. 1E). Note that the presence of branches on F-actin reduces the gliding velocity, from 50.3 ± 5.5 nm/sec for filaments without branches as we previously reported [15, 19] down to 33.1±4.8 nm/s for branched F-actin (Fig. 1F).

Sliding on Myo1b flattens the branches on the actin filaments

Since we have observed large variations of the orientation of the branches (Fig. 1C and 2A, Movies S1 and S3), we have measured the angle θ between mother and daughter filaments (Fig. 2B) on a large collection of snapshots, in the absence and in the presence of Myo1b. From the analysis of our TIRF images, we measure an average angle equal to 74±8 ° in the control conditions, in agreement with previous reports [20, 21] (Fig. 2C). In contrast, with Myo1b, the average angle decreases to 48±15°, with a large spreading of the θ values down to almost zero (Fig. 2C). This large spreading is maintained over the 5 minutes observation (Fig. 2C, blue scale), reflecting a large flexibility of the architecture of the branched filaments when sliding on Myo1b. We have also observed many instances where the branch flattens on the mother (Movies S1 and S3) and the angle decays to zero; the branch falls back towards the main filament axis in the direction opposite to the movement. Using 3D STORM, we confirmed that even when the angle is close to zero, the branch remains attached to the mother filament, and is not juxtaposed to it (Fig. 2D, Fig. S1A).
We next analyzed the architecture of the actin networks in our different experimental conditions with electron microscopy (Fig. 2E, Fig. S1B). Figure 2E shows a representative image of a branched filament in the absence of Myo1b with an angle θ=67°, of a bundle of 3 parallel filaments, and of a branch with a reduced angle in the presence of Myo1b. In average, we have observed 0.48 branches per µm (N=25 fields of 2.5 X 1.665 μm^2) without Myo1b, and 0.1 branches per µm (N=5) with Myo1b (Fig. 2F). In agreement with our time-lapse observations (Movie S2), we observe neither branches nor bundles with Myo2 (Fig. 2E).
All together, these different observations highlight the capability of Myo1b to modify the architecture of branched stabilized actin networks, to reduce the branching angle down to zero, in the direction opposite to the movement and eventually to even break the Arp2/3-mediated branch.

Sliding on Myo1b reduces branching dynamics and induces debranching.

We next investigated the effect of Myo1b on dynamical filaments that polymerize and branch using bulk pyrene-actin fluorescence or TIRF microscopy assays. As previously reported for linear F-actin, we did not observe any effect on polymerization of branched F-actin in presence of Myo1b in solution (Fig. 3A) [15]. With our TIRF assay, we observe the growth of long and straight branches along the growing mother filament in the absence of myosin, as expected. (Fig. 3B and Movie S4). In contrast, when the filaments grow while sliding on Myo1b, they appear very distorted. As previously reported in the absence of Arp2/3 [15], Myo1b also reduces the actin polymerization rate in these conditions. Using analysis of our TIRF data following [15] with 1 µM actin, 50 nM Arp2/3 et 100 nM VCA, the rate decreases from 7.37 ± 0.57 su/s (n = 60) in the absence of myosin down to 5.32 ±0.66 su/s (n= 25) with Myo1b.

Branches are formed but frequently detach and run away (Fig. 3B and Movie S4). In the presence of the same concentration of proteins and ATP, the observed number of branches formed over time is similar when sliding on Myo1b and in the control (Fig.S2A). However, the cumulated total length of F-actin is higher when the filaments slide on Myo1b than in the absence of Myo1b (Fig.S2C). We have normalized the observed branch number measured at different times by the corresponding total length of filaments. The number of branches formed per μm is time-independent but is reduced by about a factor 2 (0.11±0.02. μm^{-1}) as compared to the control (0.24±0.02.μm^{-1}) (Fig. 3C). Independently, we quantified the cumulative number of debranching events (Fig.S2B). It increases over time when sliding on Myo1b while, none occurs in the control conditions (Fig. S2B). When normalized by the total actin length (Fig. 3D), we obtain a probability of debranching equal to 0.05 ±0.01. μm^{-1}. The observed number of branches formed per μm (Fig. 3C) corresponds to the difference between the effective number of branches formed per μm (Fig. 3E) and the number of branches per μm that detach (Fig. 3D). From the measurements in Fig. 3C and Fig. 3D, we can show that the effective number of new formed branches per μm is equal to 0.16±0.02. μm^{-1}, lower than in the control (Fig. 3E). This indicates that sliding of actin filaments on Myo1b, besides reducing polymerization rate, not only induces debranching but also reduces the probability of generating new branches.

Conclusion

It is generally accepted that both types of actin networks, branched and parallel depending on the Arp2/3 complex and formin respectively, compete for the same pool of G-actin [22]. More recently it has been shown that accessory proteins such as profilin or capping protein can interfere and favor the polymerization of one or the other network [23, 24]. In this report we show that beside the accessory proteins, myosin motors, Myo1b and Myo2, also remodel the architecture of the branched actin network when attached to a substrate. This is not the case when myosins are free in solution and cannot exert forces. Bieling and colleagues [25] have suggested that compressive forces on a branched actin gel alter the internal architecture of branched actin network, increasing its density. In our experiments on stabilized and dynamical F-actin, due to the geometry of the Arp2/3-generated branch, the mother filament and the branches are propelled by myosins in divergent directions, which induces friction forces on the filaments (Fig.4). This explains the reduction of sliding velocity in the presence of branches. Moreover, the combination of the friction force (F_{fric}) on the branch due to the sliding of the mother filament and of the force produced by the motors on this branch (F_{mot}) results on a force **F** at the extremity of the filament, and thus on a torque that reduces the θ angle (Fig.4). Consequently, the Arp2/3 junction is submitted to a stress and depending on the stiffness of the Arp2/3 - F-actin junction, the branch might break either at the junction or next to it.

We have also shown that the probability of forming new branches on the side of a mother filament is reduced when sliding on myosins. Tropomyosin [4], cofilin [3] and coronin [26] inhibit the polymerization of Arp2/3-dependent actin branches by competing with the Arp2/3 complex for their binding site along F-actin. Similarly, Myo1b might compete for the same binding site with Arp2/3.

In cells, Myo1b is bound to membranes. The Ostap group and us [15, 27] have reported that even when Myo1b is bound to fluid lipid bilayers, it can propel F-actin due to the high viscosity of the membranes [15]. Thus, it is very likely that Myo1b can also debranch and reorganize the architecture of branched actin networks at the plasma membrane. This is

supported by our recent in vivo observations that Myo1b is required for the formation of filopodia induced by the stimulation of EphB2 receptors [28] and controls the extension of the branched actin network in growth cones [14]. By debranching the actin network nearby the plasma membrane, Myo1b may favor the formation of linear and parallel filaments in growth cones and facilitates the initiation of filopodia induced upon EphB2 receptors stimulation. Eventually, we showed that Myo1b can pull membrane tubules along actin bundles [19] reminiscent of the Myo1b -dependent tubule elongation at the trans Golgi network [29]. An additional role for Myo1b in this cellular region could to also debranch the Arp2/3 network, to form the structures required for it to pull tubules. Myo2 also inhibits branching actin structures. It is important to stress that this motor is not membrane-bound but associated with contractile fibers. Whether or not Myo2 *in vivo* contributes to the formation of contractile fibers by debranching Arp2/3 actin network remains to be studied.

This work, together with the former *in vivo* studies, reveals the essential role played by Myo1b in the architecture and in the dynamics of actin networks at the plasma membrane and on cellular compartments. Considering its motor activity that produces F-actin motion, we can envisage that Myo1b is also involved in general actin movements and fluxes at larger scales.

Acknowledgments

We thank B. Goud (UMR144, Institut Curie, Paris France) and J.F. Joanny (UMR168, Institut Curie, Paris France) for insightful discussions, C. Le Clainche (I2BC, Gif-sur-Yvette, France) for providing actin and actin-related proteins and for critically reading the manuscript, Anne-Sophie Mace for developing a macro to analyze the movies**,** Guillaume Romet-Lemonne and Laurent Blanchoin for carefully reading the manuscript. The authors greatly acknowledge the Cell and Tissue Imaging (PICT-IBiSA), Institut Curie, member of the French National Research Infrastructure France-BioImaging (ANR10-INBS-04). This work was supported by Institut Curie, Centre National de la Recherche Scientifique (CNRS), the European Research Council (ERC) (P.B. and E.C are partners of the advanced grant, project 33984). P.B. and E.C.'s groups belong to the CNRS consortium CellTiss, the Labex CelTisPhyBio (ANR-11-LABX0038) and Paris Sciences et Lettres (ANR-10-IDEX-0001-02). J.P. was funded by the ERC project 339847.

Author contributions

J.P., P.B and E.C. designed the study. J.P. and A.M. performed TIRF experiments and analyzed data; V.C. performed the STORM experiments and analyzed the data; A.B. performed the EM experiments; H.B. purified myosin 1b; J.P, P.B and E.C., wrote the paper.

Declaration of interests

The authors declare no competing interests.

Figures and Legends

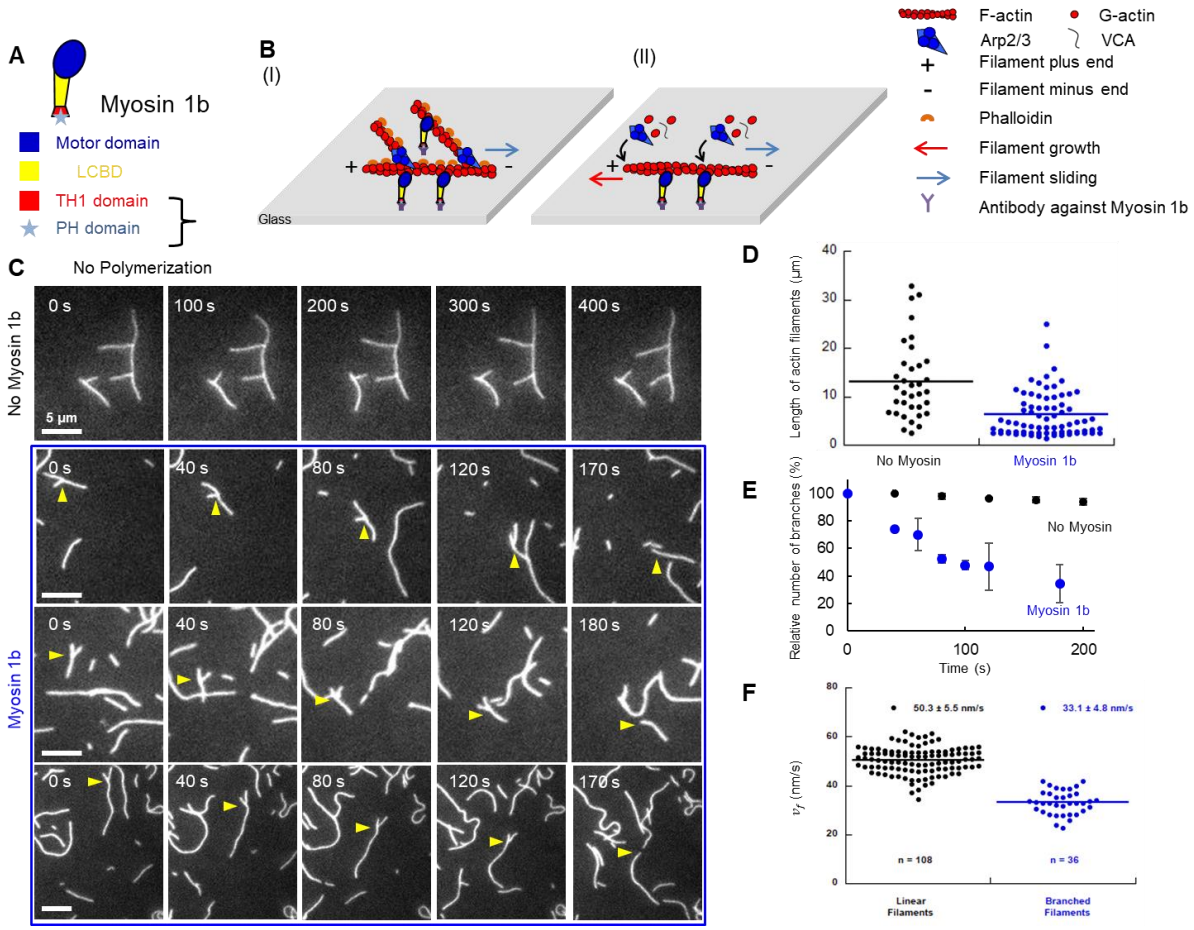

Figure 1: **Sliding on myosin 1b reduces stabilized F-actin branching. (A)** Schematic representation of domain organization of Myo1b. Motor domain (blue); Light Chain Binding Domain (LCBD) (yellow); TH1 domain (red), PH domain (cyan) that binds phosphoinositides. **(B)** Gliding assays of phalloidin-stabilized branched actin filaments (I) and polymerizing and branching actin filaments (II) sliding on Myo1b anchored on coverslip. **(C)** Time-lapse images of phalloidin-stabilized branched F-actin (prepared from 1 µM G-actin, 50 nM Arp2/3 and 100 nM VCA, see STAR Methods) in the absence of myosin or sliding on Myo1b in presence of 2 mM ATP (Movie S1). Three representative examples of branched structures in the presence of Myo1b are shown. Yellow arrows point to a single branch on the different frames. Scale bar, 5 µm. **(D)** Distribution of actin filament (mother and attached branches) lengths at t=160 s, in one field corresponding to Movie S1 (no myosin and 2nd from left). **(E)** Relative number of branches along actin filaments (STAR Methods) normalized by the number of branches N_0 at t=0, as a function of time in the absence of myosin (N_0=60, two movies) or sliding on Myo1b (N_0=38, two movies). **(F)** Dot plot representation of sliding velocities v_f of stabilized actin filaments in the presence of Arp2/3, showing or not branches. The number of analyzed filaments and the mean-values ± s.e.m. are indicated.

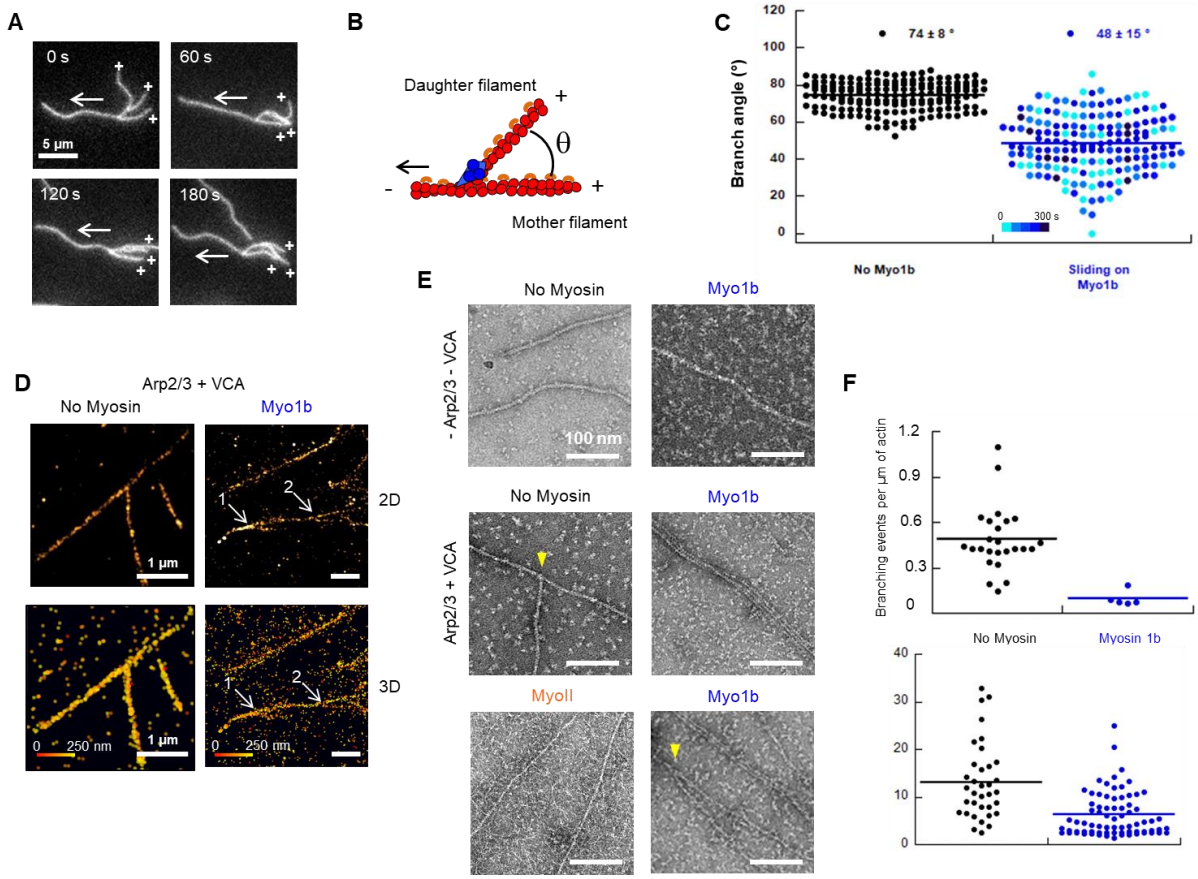

Figure 2: Myosin 1b reduces stabilized F-actin angles in branched structures. (A) Time-lapse images of stabilized branched F-actin, (prepared from 1 µM G-actin, 50 nM Arp2/3 and 100 nM VCA, see STAR Methods) sliding on Myo1b in presence of 2 mM ATP, showing a change of the angle between mother and daughter filaments (Movie S3). Crosses indicate barbed ends and the white arrow corresponds to the sliding direction. Scale bar, 5 µm. **(B)** Representation of the angle θ between mother and daughter filaments. **(C)** Dot plot representation of the angle between mother and daughter filaments in the absence of myosin (12 filaments, 168 images) or sliding on Myo1b (19 filaments, 168 images), in the same experimental conditions as described in Fig. 2. Blue scale indicates the time since the beginning of the acquisition. **(D)** STORM images of stabilized branched F-actin in 2D (**top**) or 3D (**bottom**) in the absence or in the presence of Myo1b and 2 mM ATP. These images are magnification of part of the corresponding large field views shown in Fig. S1A. The color code from red to yellow indicates the height (z). In the absence of Myo1b, the branch and the mother filaments are in the same plane and attached. On Myo1b, branches #1 and #2 exhibit an angle with the mother filament much lower than 70°, but are physically connected to it. Note that branch #2 is in a lower plane **(E)** Electron microcopy images after negative staining. Images of stabilized F-actin prepared from 4 µM G-actin, branched or not, were recorded after gliding 10 min or not on Myo1b or Myo2 at 2 mM ATP. These images are magnification of part of the corresponding large field views shown in Fig. S1B. Scale bars, 100 nm. **(F)** Dot plot representing the number of branches per µm of actin, in the absence of myosin or sliding on Myo1b

Figure 3

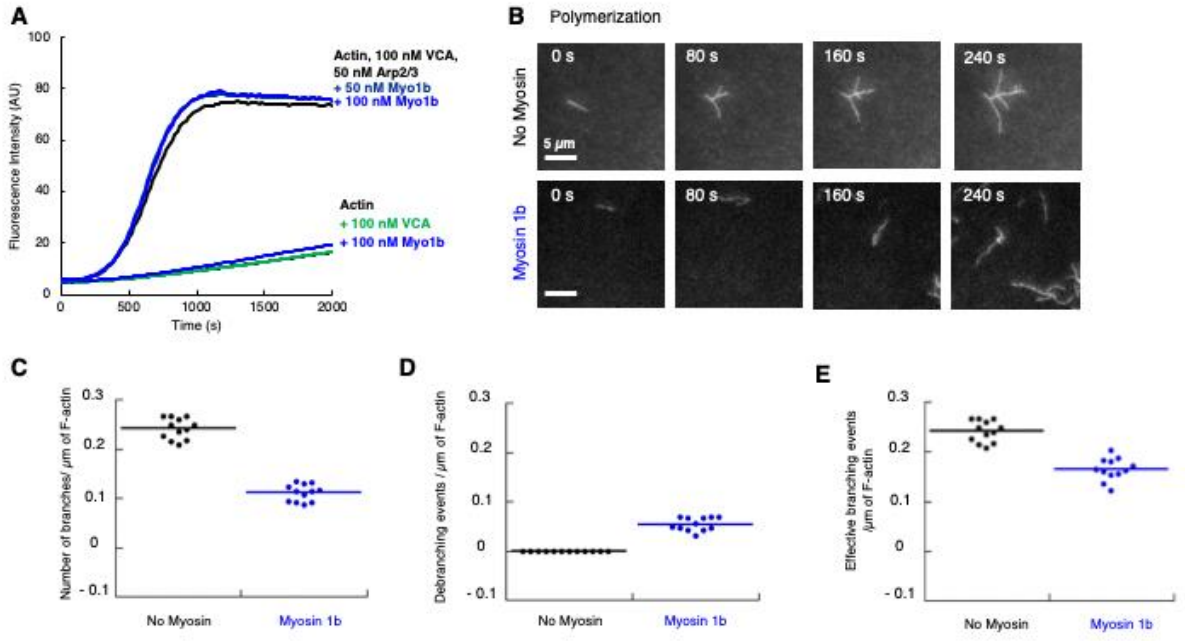

Figure 3: **Sliding on myosin 1b decreases branching of polymerizing actin filaments. (A)** Effect of Myo1b on branched F-actin polymerization using pyrene assay (in the presence of 100 nM VCA and 50 nM Arp2/3, 2 µM actin, 10% pyrenyl-labeled). **(B)** Time-lapse images of polymerizing and branching F-actin in the absence of myosin or sliding on Myo1b at 2 mM ATP (Movie S4). Scale bar, 5 µm. **(C)** Numbers of branches per µm of F-actin, in the absence of myosin or sliding on Myo1b. They are obtained from the total number of branches detected at different times (Fig. S2A) normalized by the corresponding total actin length (Fig. S2C). **(D)** Numbers of debranching events per µm of F-actin, in the absence of myosin or sliding on Myo1b, obtained from the total number of debranching events detected at different times (Fig. S2B) normalized by the corresponding total actin length (Fig. S2C). **(E)** Effective branching events per µm of F-actin, calculated from the sum of the observed branches number (C) and debranching events (D), in the absence of myosin or sliding on Myo1b. (C), (D) and (E) correspond to data from three different fields of 80x80 µm^2 (see Fig. S2).

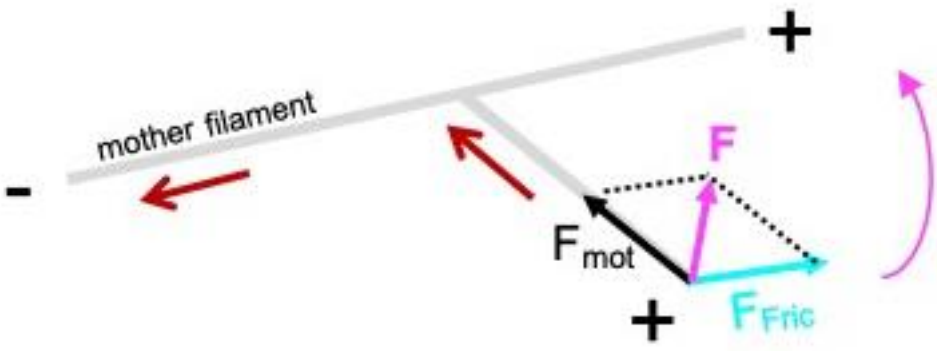

Figure 4: Schematic representation of the forces exerted on a daughter filament.
Mother filament sliding (red arrow) induces a friction force (F_{fric}) on the daughter filament. F_{fric} combined to the force generated by the motors on the branch (F_{mot}) results in a total force ***F*** at the extremity of the filament and thus in a torque leading to the reduction of the angle between both filaments (magenta arrow).

Supplemental Information

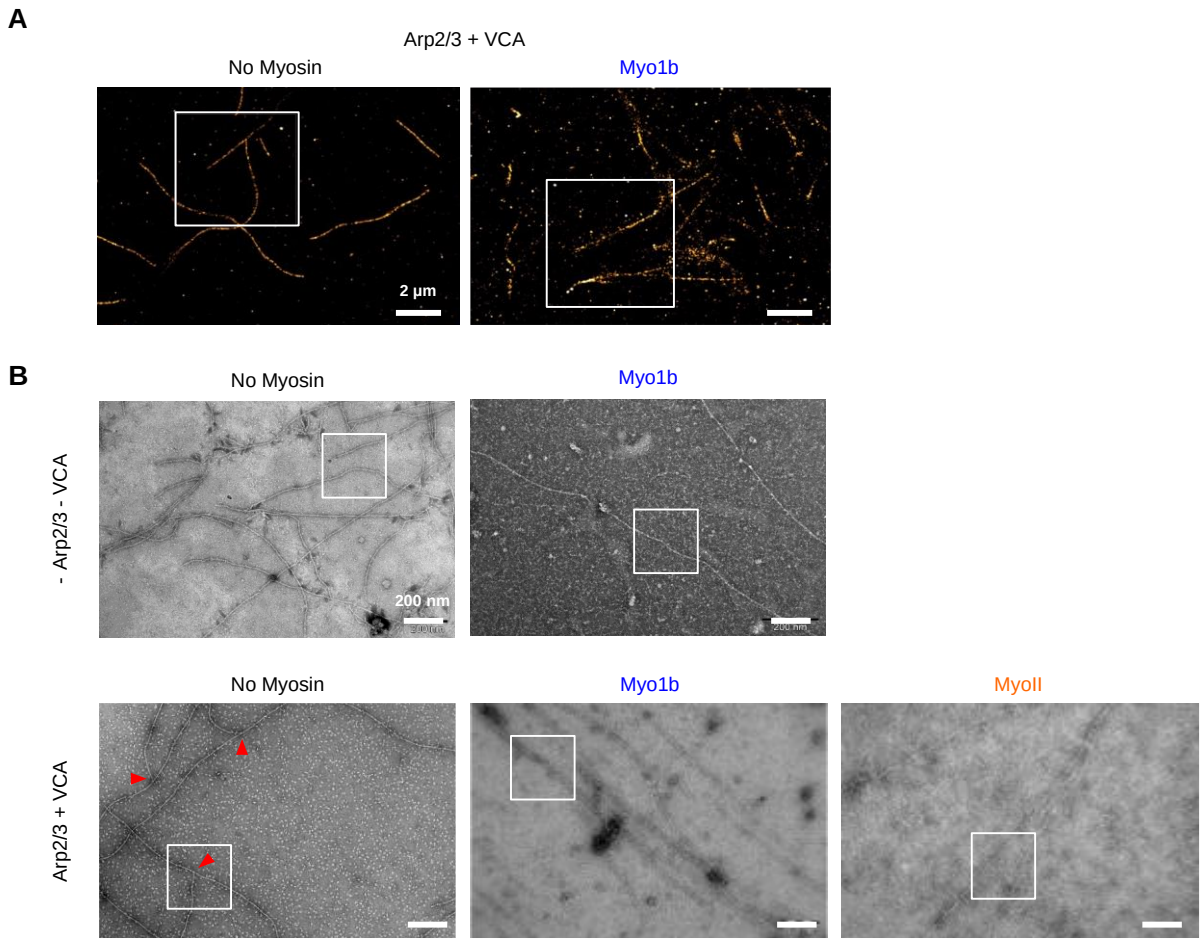

Figure S1: Large fields corresponding to the zooms (white frames) shown: (A) in Fig. 3D with STORM and (B) in Fig. 3E with electron microscopy. In (B), red triangles indicate branched junctions. Scale bars 2 µm (A) and 200 nm (B).

Figure S2

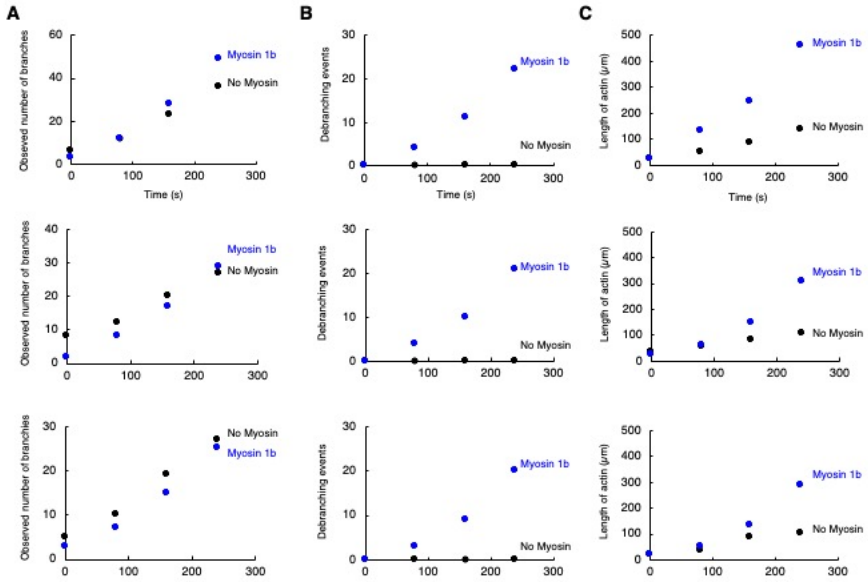

Figure S2: Data corresponding to Fig. 3C and 3D. (A) Observed number of branches, **(B)** total debranching events, **(C)** total length of actin, over time and on three different fields of 80x80 μm^2.

Movie S1: Stabilized branched actin filaments sliding along glass-anchored myosin 1b (corresponding to Fig. 2).

Branched filaments stabilized with phalloidin-Alexa547 in the absence of myosin (left) or sliding on Myo1b at high density (8000 μm^{-2}). Scale bar 5 µm. Time in s. Wide field movies corresponding to time-lapse images shown in Fig. 1C.

Movie S2: Stabilized branched actin filaments sliding along myosin II.

Branched filaments stabilized with phalloidin-Alexa547 sliding on Myo2. The movie starts 1 min after injection of branched filaments in the chamber. Scale bar, 5 µm. Time in s.

Movie S3: Effect of myosin 1b on organization of branched structures (corresponding to Fig. 2A).

Branched filaments stabilized with phalloidin-Alexa547 sliding on Myo1b. Scale bar, 5 µm. Time in s.

Movie S4: Polymerizing and branching actin filaments sliding along glass-anchored Myo1b (corresponding to Fig. 3).

Polymerized and branched actin filaments in the absence of myosin or sliding on Myo1b at high density (8000 μm^{-2}). Scale bar, 5 µm. Time in s. Wide field movies corresponding to time-lapse images shown in Fig. 3B. The appearance over time of new actin filaments on the right side of the movie likely results from the high affinity of these filaments for the surface coated with Myo1b.

STAR Methods

Protein purification

Actin was purified from rabbit muscle and isolated in monomeric form in G buffer (5 mM Tris-HCl, pH 7.8, 0.1 mM $CaCl_2$, 0.2 mM ATP, 1 mM DTT and 0.01% NaN_3). Actin was labeled with Alexa 594 succimidyl ester-NHS [30].

Myosin II was purified from rabbit muscle as previously described [31].

Arp2/3complex was purified from bovine brain [32].

Expression and purification of Myosin 1b: FLAG-myo1b was expressed in HEK293-Flp-In cells cultured in Dulbecco's modified Eagle medium supplemented with 10% fetal bovine serum and 0.18 mg ml^{-1} hygromycine in a spinner flask at 37 °C under 5% CO_2, and collected by centrifugation (1,000 g, 10min, 4 °C) to obtain a 4–5 g of cell pellet. The pellet was lysed in FLAG Trap binding buffer (30 mM HEPES, pH 7.5, 100 mM KCl, 1 mM $MgCl_2$, 1mM EGTA, 1 mM ATP, 1 mM DTT, 0.1% protease inhibitor cocktail (PIC), 1% Triton X-100) for 30 min at 4 °C and centrifuged at 3,400 g for 10 min at 4 °C. The collected supernatant was then ultracentrifuged (250,000 g, 60 min, 4 °C). The solution between pellet and floating lipid layer was incubated with 150 µl of anti-FLAG beads for 2 h at 4 °C. The beads were collected by centrifugation (1,000 g, 5 min, 4 °C). After a washing step, FLAG-myo1b was then eluted by incubating with 0.24 mg ml^{-1} of 3X FLAG peptide in 300 µl elution buffer (binding buffer without Triton X-100 supplemented with 0.1% methylcellulose) for 3 h at 4 °C. After removal of the beads by centrifugation (1,000 g, 3 min, 4 °C), the protein solution was dialyzed against elution buffer overnight at 4 °C to remove the 3X FLAG peptide. Myo1b was fluorescently labeled using Alexa Fluor 488 5-SDP ester [19]. Inactivated Myo1b was removed by ultracentrifugation (90,000 rpm, 20 min, 4 °C) with 10 µM F-actin in presence of 2 mM ATP. Inactivated Myo1b was then dissociated from F-actin by incubating the pellet collected after untracentrifugation in elution buffer (30 mM HEPES, pH 7.5, 100 mM KCl, 1 mM $MgCl_2$, 1mM EGTA, 1 mM ATP, 1 mM DTT and 0.1% methylcellulose) supplemented with 1 M NaCl and collected in the supernatant after a second centrifugation (90,000 rpm, 20 min, 4 °C).

Actin polymerization assays

Actin polymerization kinetic experiments were based on fluorescence change of pyrenyl-labeled G-actin (λ_{exc}=365 nm, λ_{em}=407 nm). Experiments were carried out on a Safas Xenius spectrofluorimeter (Safas, Monaco).

Polymerization assays were performed in F-buffer (5 mM Tris-HCl, pH 7.8, 100 mM KCl, 1 mM $MgCl_2$, 0.2 mM EGTA, 0.2 mM ATP, 1 mM DTT, 0.01% NaN_3) in the presence of 100 nM VCA, 50 nM Arp2/3 and 2 µM Actin 10% pyrenyl-labeled).

TIRF microscopy assays and data analysis

The kinetics of single filament assembly Coverslips and glass slides were sequentially cleaned by sonication with H_2O, ethanol, acetone for 10 min, then 1M KOH for 20 min and H_2O for 10 min. Flow chambers were assembled with a coverslip bound to a glass slide with two parallel double-stick tapes. The chamber was incubated with 100 nM anti-myo1b antibody in G buffer (5 mM Tris-HCl, pH 7.8, 0.1 mM $CaCl_2$, 0.2 mM ATP, 1 mM DTT and 0.01% NaN_3) for 10 min at room temperature. The chamber was rinsed three times with buffer G 0.1 % BSA and incubated 5 min at room temperature. Then the chamber was incubated with 300 nM Alexa488-labeled myo1b in Fluo F buffer (5 mM Tris-HCl, pH 7.8, 100 mM KCl, 1 mM $MgCl_2$, 0.2 mM EGTA, 0.2 mM or 2 mM ATP, 10 mM DTT, 1 mM DABCO, 0.01% NaN_3) for 10 min at room temperature. Actin gliding assays were performed in Fluo F buffer, containing ATP

maintained constant at 2 mM with a regenerating mix (see below), supplemented with 0.3% methylcellulose (Sigma) and with G-actin (1µM, 10% Alexa594-labelled), VCA and Arp2/3 complex or stabilized branched F-actin (stabilized with phalloidin-Alexa594) prepared as below. Actin was polymerized in the presence of 100 nM VCA and 50 nM of Arp2/3 complex. In the case of stabilized filaments, after 10 min. samples were diluted 20-fold to 50 nM and supplemented with phalloidin. The dynamic of stabilized branched filaments and polymerizing and branching actin filaments was monitored by TIRF microscopy (Eclipse Ti inverted microscope, 100X TIRF objectives, Quantem 512SC camera). The experiments were controlled using the Metamorph software. To maintaining a constant concentration of ATP in this assay an ATP regenerating mix, including 2 mM ATP, 2 mM $MgCl_2$, 10 mM creatine phosphate and 3.5 U/mL creatine phosphokinase, which constantly re-phosphorylates ADP into ATP to maintain a constant concentration of free ATP, was added.
The sliding velocities of actin filaments were analyzed by using Kymo Tool Box plugin of Image J software (https://github.com/fabricecordelieres/IJ_KymoToolBox). The accuracy on the displacement of the filaments is of the order of the pixel size (160 nm). The number of branches and the length of the filaments were measured by using Analyze Skeleton plugin in Image J (https://imagej.net/AnalyzeSkeleton) on transformed movies obtained by running an automatic macro
(freely accessible on: http://xfer.curie.fr/get/SItjDQoyu4k/automatization_skeleton.ijm)

STORM
Stabilized branched F-actin in the absence of myosin or after 10 min of sliding on Myo1b was visualized by incubation with phalloidin-Alexa647. Samples were mounted in dSTORM buffer (Abbelight, Paris, France). Then, 3D nanoscopy images were taken using a SAFe360 module (Abbelight) coupled to the camera port of an inverted bright-field Olympus IX71 microscope, equipped with a 100×oil-immersion objective with a high numerical aperture (NA; 1.49). This quad-view system (dual-cam sCMOS cameras, Orcaflash v4, Hamamatsu) provided 3D nanoscopy information with high isotropic localization precision (15×15×15 nm, over an axial range of~1 mm). Axial information was obtained by super-critical angle fluorescence (SAF) and the point spread function (PSF) deformation with a strong astigmatism (DAISY) (Cabriel et al., 2018). Twenty-thousand frames at 50 ms were acquired to collect the single-molecule detections and reconstruct a nanoscopy image. Resulting coordinate tables and images were processed and analyzed using SAFe NEO software (Abbelight).

Electron microscopy
4 µL of Myo1b or Myo2 samples was incubated on glow discharged and carbon coated electron microscopy grids (CF-300, EMS). After rinsing with the actin buffer, stabilized F-actin in the presence of Arp2/3 and VCA, was incubated on the grid at 2 mM ATP. The sample was thereafter stained with 4 µL uranyl formate 2%. Images were collected with a Tecnai Spirit transmission electron microscope equipped with a LaB6 emission filament operated at an acceleration voltage of 80 kVolts (Thermofischer, FEI, Eindhoven, The Netherlands). The microscope is equipped with a Quemesa (Olympus) camera for imaging.

References

1. Blanchoin, L., Boujemaa-Paterski, R., Sykes, C., and Plastino, J. (2014). Actin Dynamics, Architecture, and Mechanics in Cell Motility. Physiol. Rev. *94*, 235-263.
2. Pernier, J., Shekhar, S., Jegou, A., Guichard, B., and Carlier, M.-F. (2016). Profilin interaction with actin filament barbed end controls dynamic instability, capping, branching, and motility. Dev. Cell *36*, 201-214.
3. Chan, C., Beltzner, C.C., and Pollard, T.D. (2009). Cofilin Dissociates Arp2/3 Complex and Branches from Actin Filaments. Curr. Biol. *19*, 537-545.
4. Blanchoin, L., Pollard, T.D., and Hitchcock-DeGregori, S.E. (2001). Inhibition of the Arp2/3 complex-nucleated actin polymerization and branch formation by tropomyosin. Curr. Biol. *11*, 1300-1304.
5. Reymann, A.-C., Boujemaa-Paterski, R., Martiel, J.-L., Guérin, C., Cao, W., Chin, H.F., De La Cruz, E.M., Théry, M., and Blanchoin, L. (2012). Actin Network Architecture Can Determine Myosin Motor Activity. Science *336*, 1310-1314.
6. Loubéry, S., Delevoye, C., Louvard, D., Raposo, G., and Coudrier, E. (2012). Myosin VI Regulates Actin Dynamics and Melanosome Biogenesis. Traffic *13*, 665-680.
7. Ripoll, L., Heiligenstein, X., Hurbain, I., Domingues, L., Figon, F., Petersen, K.J., Dennis, M.K., Houdusse, A., Marks, M.S., Raposo, G., et al. (2018). Myosin VI and branched actin filaments mediate membrane constriction and fission of melanosomal tubule carriers. J. Cell Biol. *217*, 2709–2726.
8. Nagy, S., Ricca, B.L., Norstrom, M.F., Courson, D.S., Brawley, C.M., Smithback, P.A., and Rock, R.S. (2008). A myosin motor that selects bundled actin for motility. Proc. Natl Acad. Sci. USA *105*, 9616-9620.
9. Schietroma, C., Yu, H.-Y., Wagner, M.C., Umbach, J.A., Bement, W.M., and Gundersen, C.B. (2007). A role for myosin 1e in cortical granule exocytosis in Xenopus oocytes. J. Biol. Chem. *282*, 29504-29513.
10. Sokac, A.M., Schietroma, C., Gundersen, Cameron B., and Bement, W.M. (2006). Myosin-1c Couples Assembling Actin to Membranes to Drive Compensatory Endocytosis. Dev. Cell *11*, 629-640.
11. Yu, H.-Y.E., and Bement, W.M. (2007). Multiple myosins are required to coordinate actin assembly with coat compression during compensatory endocytosis. Mol. Biol. Cell *18*, 4096-4105.
12. Idrissi, F.-Z., Wolf, B.L., and Geli, M.I. (2002). Cofilin, But Not Profilin, Is Required for Myosin-I-Induced Actin Polymerization and the Endocytic Uptake in Yeast. Mol. Biol. Cell *13*, 4074-4087.
13. Geli, M.I., Lombardi, R., Schmelzl, B., and Riezman, H. (2000). An intact SH3 domain is required for myosin I-induced actin polymerization. EMBO J. *19*, 4281-4291.
14. Iuliano, O., Yoshimura, A., Prospéri, M.-T., Martin, R., Knölker, H.-J., and Coudrier, E. (2018). Myosin 1b promotes axon formation by regulating actin wave propagation and growth cone dynamics. J. Cell Biol. *217*, 2033.
15. Pernier, J., Kusters, R., Bousquet, H., Lagny, T., Morchain, A., Joanny, J.-F., Bassereau, P., and Coudrier, E. (2019). Myosin 1b is an actin depolymerase. Nat. Commun. *10*, 5200.
16. McIntosh, B.B., and Ostap, E.M. (2016). Myosin-I molecular motors at a glance. J. Cell Sci. *129*, 2689-2695.

17. Komaba, S., and Coluccio, L.M. (2010). Localization of Myosin 1b to Actin Protrusions Requires Phosphoinositide Binding. J. Biol. Chem. *285*, 27686-27693.
18. Laakso, J.M., Lewis, J.H., Shuman, H., and Ostap, E.M. (2008). Myosin I can act as a molecular force sensor. Science *321*, 133-136.
19. Yamada, A., Mamane, A., Lee-Tin-Wah, J., Di Cicco, A., Prévost, C., Lévy, D., Joanny, J.-F., Coudrier, E., and Bassereau, P. (2014). Catch-bond behaviour facilitates membrane tubulation by non-processive myosin 1b. Nat. Commun. *5*, 3624.
20. Svitkina, T.M., and Borisy, G.G. (1999). Arp2/3 complex and actin depolymerizing factor/cofilin in dendritic organization and treadmilling of actin filament array in lamellipodia. J. Cell Biol. *145*, 1009-1026.
21. Mullins, R.D., Heuser, J.A., and Pollard, T.D. (1998). The interaction of Arp2/3 complex with actin: nucleation, high affinity pointed end capping, and formation of branching networks of filaments. Proc. Natl Acad. Sci. USA *95*, 6181-6186.
22. Chesarone, M.A., and Goode, B.L. (2009). Actin nucleation and elongation factors: mechanisms and interplay. Curr. Opin. Cell Biol. *21*, 28-37.
23. Rotty, Jeremy D., Wu, C., Haynes, Elizabeth M., Suarez, C., Winkelman, Jonathan D., Johnson, Heath E., Haugh, Jason M., Kovar, David R., and Bear, James E. (2015). Profilin-1 Serves as a Gatekeeper for Actin Assembly by Arp2/3-Dependent and -Independent Pathways. Dev. Cell *32*, 54-67.
24. Suarez, C., Carroll, R.T., Burke, T.A., Christensen, J.R., Bestul, A.J., Sees, J.A., James, M.L., Sirotkin, V., and Kovar, D.R. (2015). Profilin regulates F-actin network homeostasis by favoring formin over Arp2/3 complex. Dev. Cell *32*, 43-53.
25. Bieling, P., Li, T.-D., Weichsel, J., McGorty, R., Jreij, P., Huang, B., Fletcher, Daniel A., and Mullins, R.D. (2016). Force Feedback Controls Motor Activity and Mechanical Properties of Self-Assembling Branched Actin Networks. Cell *164*, 115-127.
26. Cai, L., Makhov, A.M., Schafer, D.A., and Bear, J.E. (2008). Coronin 1B antagonizes cortactin and remodels Arp2/3-containing actin branches in lamellipodia. Cell *134*, 828-842.
27. Pyrpassopoulos, S., Feeser, E.A., Mazerik, J., Tyska, M., and Ostap, M. (2012). Membrane-bound Myo1c powers asymmetric motility of actin filaments. Curr. Biol. *22*, 1688-1692.
28. Prospéri, M.-T., Lépine, P., Dingli, F., Paul-Gilloteaux, P., Martin, R., Loew, D., Knölker, H.-J., and Coudrier, E. (2015). Myosin 1b functions as an effector of EphB signaling to control cell repulsion. J. Cell Biol. *210*, 347-361.
29. Almeida, C.G., Yamada, A., Tenza, D., Louvard, D., Raposo, G., and Coudrier, E. (2011). Myosin 1b promotes the formation of post-Golgi carriers by regulating actin assembly and membrane remodelling at the trans-Golgi network. Nat. Cell Biol. *13*, 779-789.
30. Ciobanasu, C., Faivre, B., and Le Clainche, C. (2014). Actomyosin-dependent formation of the mechanosensitive talin–vinculin complex reinforces actin anchoring. Nat. Commun. *5*, 3095.
31. Pollard, T.D. (1982). Myosin Purification and Characterization. In Method Cell Biol., Volume 24, L. Wilson, ed. (Elsevier Inc.), pp. 333-371.
32. Egile, C., Loisel, T.P., Laurent, V., Li, R., Pantaloni, D., Sansonetti, P.J., and Carlier, M.-F. (1999). Activation of the CDC42 effector N-WASP by the Shigella flexneri IcsA protein promotes actin nucleation by Arp2/3 complex and bacterial actin-based motility. J. Cell Biol. *146*, 1319.